GLOBAL DRAG OF HETEROGENEOUS SURFACES WITH VARYING REYNOLDS NUMBER

C. Schmidt[1], *P. Sujar-Garrido*[2,1], *R. Leister*[3], *J. Kriegseis*[1], *D. Gatti*[1] *and B. Frohnapfel*[1]

[1] *Institute of Fluid Mechanics (ISTM), Karlsruhe Institute of Technology (KIT) 76131 Karlsruhe, Germany*

[2] *FLOW, Dept. Engineering Mechanics, KTH Royal Institute of Technology 100 44 Stockholm, Sweden*

[3] *Institute for Modelling Hydraulic and Environmental Systems (IWS), University of Stuttgart 70569 Stuttgart, Germany*

carola.schmidt@kit.edu

Abstract

The influence of the distinct distribution of rough surface parts on the friction coefficient of heterogeneous rough surfaces is investigated experimentally in a wide Reynolds number range. The effects of a checkerboard-patterned surface are compared to a surface with streamwise-aligned roughness strips. The effects the roughness distributions have on the flow field are investigated further by hot-wire anemometry and Lagrangian particle tracking velocimetry.

1 Introduction

Many surfaces exposed to (turbulent) flows are heterogeneously rough as for example ship hulls overgrown with barnacles or locally corroded pipelines. Especially for technical surfaces, the global drag is of high interest, but its prediction remains challenging (Chung *et al.* (2021)). Existing suggestions for predictive tools are based on the assumption of constant statistical properties of the surface parts over large areas and the flow being in equilibrium with the underlying surface condition (see e.g. Bou-Zeid *et al.* (2020), Neuhauser *et al.* (2022), Hutchins *et al.* (2023)). Edge effects are neglected and in consequence, the predictions take the percentage of the surface covered with roughness into account, but not the discrete distribution of the roughness parts. However, it has already been shown that the spatial distribution of the roughness influences the global drag of the surface, even if the roughness coverage ratio is constant (Frohnapfel *et al.* (2024), Neuhauser *et al.* (2025)).

The present work aims at shedding more light on the influence of the arrangement of the rough surface parts onto the global drag. It is supposed to widen the data base of reference data to enhance the possibility of validation and improvement of the existing predictive tools. Therefore, different roughness arrangements are investigated in a blower-type wind tunnel in a wide Reynolds number range.

2 Investigated surfaces

Two heterogeneous surface configurations are investigated to shed more light on the link between the global friction coefficient, discrete roughness distribution and Reynolds number. In both configurations, the roughness consists of P60 sandpaper and the surface portion covered with roughness is kept constant at $50\,\%$. In order to avoid problems in the data evaluation stemming from differing channel height, the surfaces are produced such that the roughness mean height is at the same elevation height as the smooth surface parts as is sketched e.g. in Figure 1. To complement the data of the heterogeneous surfaces, the global drag of the respective homogeneous surfaces, i.e. smooth and rough, is measured.

The first investigated surface consists of alternating smooth and rough strips with a width of $4\,\delta$ oriented in parallel to the mean flow direction, with δ being the half channel height of the test section. Such surfaces consisting of streamwise strips are called strip-type surfaces. Existing studies investigating such strip-type surfaces focussed on the formation of secondary motions of Prandtl's second kind induced by the spanwise transition from smooth to rough and *vice versa* (see e.g. Hinze (1967), Vanderwel and Ganapathisubramani (2015)). The studies were either carried out in turbulent boundary layers (e.g. Anderson *et al.* (2015), Wangsawijaya *et al.* (2020)), or in channel flow (Neuhauser *et al.* (2025)). However, the corresponding global drag and its dependence on Reynolds number has rarely been discussed in the literature.

The obtained data from the $4\,\delta$ surface are compared to those of a surface with added streamwise heterogeneity. The wide strips are regularly inter-

rupted, resulting in a checkerboard-like pattern composed from squares with $4\,\delta$ side length. Principle sketches of the two surface configurations can be seen on the right side of Figure 4.

Existing investigations of streamwise changes in surface condition, *i.e.* smooth-to-rough and *vice versa*, focus on the recovery length needed until the flow reaches a new equilibrium with the underlying surface condition. The corresponding studies were carried out in boundary layers (see e.g. Antonia and Luxton (1971), Hanson and Ganapathisubramani (2016)) and the recovery length is found to be in the order of $20 - 50\,\delta$ (Devenport and Lowe (2022)). Over this distance an internal boundary layer which reflects the new surface conditions grows until it fully replaces the original boundary layer. In addition, over- and undershooting of the friction coefficient has been observed after the step change. To the author's knowledge there is no systematic study on the Reynolds number dependence of the growth of the internal boundary layer and the respective wall shear stress development. The checkerboard surface pattern is likely to contain both types of flow effects, i.e. the ones related to spanwise and to streamwise step changes in boundary condition.

3 Experimental set-up

Channel flow facility

The experimental investigation to obtain the friction coefficient for different surfaces is carried out in the blower-type wind tunnel depicted in Figure 2. The test section which is placed downstream of the settling chamber has a width of $W = 300\,\mathrm{mm}$ and a half-height of $\delta = 12.6\,\mathrm{mm}$, resulting in an aspect ratio of $AR = 12$. The overall length of the test section is about $4\,\mathrm{m}$ corresponding to $314\,\delta$. The investigated surfaces are placed after a development length of almost $200\,\delta$ symmetrically on the top and bottom walls within the last part of the test section. This principal configuration including the geometrical definitions is sketched in Figure 1. The test section is equipped with 21 pairs of pressure taps placed in regular intervals of $200\,\mathrm{mm}$ along the side walls. The taps along the structured surfaces, starting $20\,\delta$ behind the leading edge of the rough surface, are used to obtain the streamwise pressure gradient Π.

In order to measure the mass flow rate $\dot{m}$ an orifice meter is installed on the suction side of the fan. To capture the wide Reynolds number range of $4500 < Re_b < 85000$ the plates installed in the orifice flow meter are changed several times during the measurement campaign to maintain the pressure drop within the measurement range of the installed pressure sensors.

Hot-wire Anemometry

A DANTEC 55P11 single wire probe equipped with a tungsten wire with a diameter of $0.5\,\mathrm{mm}$ and a sensing length of $1.25\,\mathrm{mm}$ is used to measure the streamwise velocity at $Re_b = 18000$. The streamwise

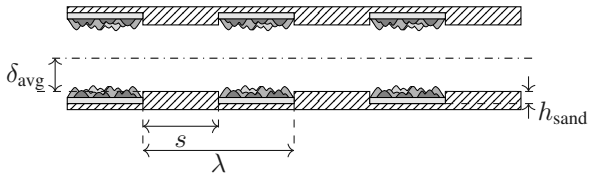

Figure 1: Principal sketch of the investigated surfaces as they are mounted symmetrically as top and bottom plate of the test section. The average channel height δ, strip width or side length s, respectively, and wavelength $\lambda = 2s$ as well as the roughness mean height (including the sandpaper's base material) h_{sand} are labelled.

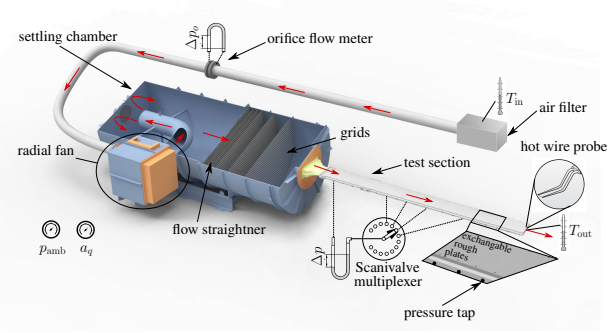

Figure 2: Schematic of the utilized wind tunnel including measurement instrumentation (adapted from Frohnapfel *et al.* (2024)).

location is fixed to $1 - 1.5\,\mathrm{cm}$ upstream of the test section outlet whilst the spanwise and wall-normal position are varied by means of a two-axis traversing system. The probe is operated by a DANTEC Streamline Pro frame in conjunction with a 90C10 constant temperature anemometer (CTA) system at a fixed overheat ratio of $80\,\%$. An offset and gain are chosen appropriate to the A/D converter used and applied to the raw signal. The sampling time is set to $18\,\mathrm{s}$, the sampling frequency to $60\,\mathrm{kHz}$ combined with a low-pass filter of $30\,\mathrm{kHz}$. The velocity calibration is performed *ex-situ* in a pressure driven jet before and after the measurements. Temperature changes during the run are recorded and accounted for by a temperature compensation as outlined in Örlü & Vinuesa (2017).

Volumetric Shake-the-Box measurements

Volumetric Shake-the-Box (STB) measurements are performed to capture the spanwise and streamwise evolution of the flow, utilizing a thin laser light volume positioned above the lower channel wall to enable particle tracking near the wall. A window in the upper channel wall provides optical access for four cameras in pyramidal arrangement, capturing the particles in the flow under Scheimpflug conditions. These experi-

ments are carried out in a second blower-type channel flow facility, which is a replica of the one introduced previously. For more details on this facility regarding inlet conditions and Reynolds definitions the reader is referred to Hehner *et al.* (2022) and Pasch *et al.* (2024).

The reconstructed volume, $18\,\mathrm{mm} \times 5\,\mathrm{mm} \times 10\,\mathrm{mm}$ in main flow direction (x), wall-normal direction (y), and spanwise direction (z), covers a region above a pair of smooth-rough patches (Top Figure 3). While transparent walls allow STB flow resolution down to the viscous sublayer despite the small facility channel height at $Re_\tau = 350$ (Kriegseis *et al.* (2024)), reflections from the opaque sandpaper surface pose additional challenges. To mitigate this, the final volume is located slightly further from the wall and cropped to exclude outliers and ghosts particles.

Velocity fields were extracted using DaVis 11 (*LaVision*) Shake-the-Box evaluation (Schanz *et al.* (2016)). Each measurement lasts 1 second at an acquisition frequency of 30 kHz. Bottom Figure 3 illustrates instantaneous flow with the centreline velocity being $U_{\mathrm{cl}} = 8.5\,\mathrm{m\,s^{-1}}$. The flow direction is towards positive x-values, represented by the black arrow and the wall normal coordinate $y = 0$ marks the estimated plate position determined via the calibration target on a micrometer traverse system.

4 Results

In a first step, the results are presented in terms of the global friction coefficient C_f as a function of the channel's bulk Reynolds number Re_b. The two quantities need to be determined from the measured quantities which are the mass flow rate $\dot{m}$, the pressure gradient along the test surface $\Pi = -\frac{\Delta p}{\Delta x}$, the air's density ρ and viscosity ν as well as the geometric dimensions, *i.e.* the tunnel width W and half channel height δ. This results in

$$Re_b = \frac{2\delta U_b}{\nu} = \frac{\dot{m}}{\rho \nu W} \tag{1}$$

for the Reynolds number, and

$$C_f = \frac{2\tau_w}{\rho U_b^2} = \frac{8\Pi\rho\delta^3 W^2}{\dot{m}^2} \tag{2}$$

for the friction coefficient.

The obtained results of the homogeneous and heterogeneous surfaces are shown in Figure 4. To account for the different orifice plates the results are represented using a unique symbol per orifice plate.

Both curves of the heterogeneous surfaces are placed between the two homogeneous curves. Even though both surfaces are covered with the same amount of roughness, it can be seen on first glance that they show different drag behaviour stemming from the different roughness distributions. The flow above the checkerboard pattern experiences less drag than above the strip-type surface, especially in the low Reynolds

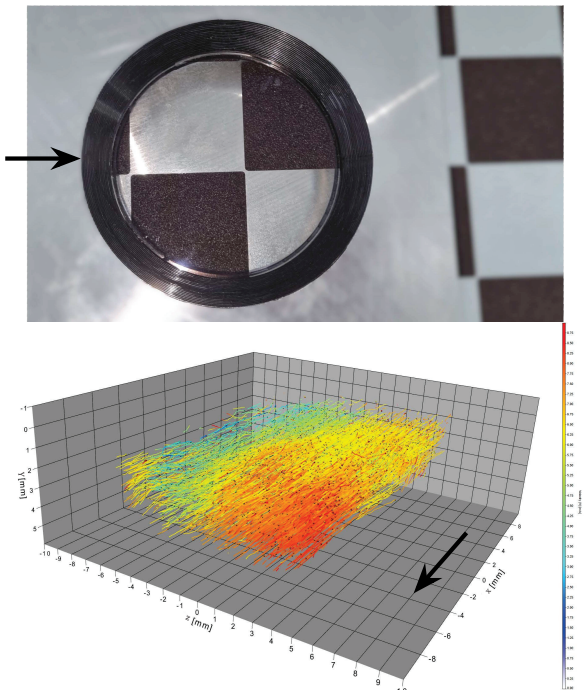

Figure 3: Principal view of the window in the upper channel wall showing the optical access for the four cameras (top). The final field of view is a cropped version of this view. Example of instantaneous STB, high- and low-speed regions can be distinguished (bottom). In both cases, black arrows indicate the streamwise flow direction.

number regime of our facility. At high Reynolds numbers, the difference between the two surfaces vanishes. To enable not only a qualitative but also quantitative comparison, the relative difference of the checkerboard's friction coefficient to the strip-type surface's friction coefficient

$$\Delta C_{f,c\to s} = \frac{C_{f,\mathrm{check}} - C_{f,\mathrm{strip}}}{C_{f,\mathrm{strip}}} \tag{3}$$

is calculated and plotted in Figure 5. In the low Reynolds number range we observe a "drag reduction" effect which reaches its maximum around $Re_b \approx 12000$ with a relative drag difference of $-10\,\%$. At high Reynolds numbers, the difference between the two surfaces vanishes to less than $1\,\%$ and is therefore negligible.

In order to better understand the behaviour at low Reynolds numbers, the velocity fields above the two surfaces are investigated around the Reynolds number of the highest difference in drag. Two different measurement techniques are employed in this context. As the strip-type surface is invariant in streamwise direction, the velocity is measured at a fixed streamwise position in a wall-normal plane at $Re_b = 18000$ by means of hot-wire anemometry. The measurements are conducted as close to the spanwise centre of the channel as possible, enabling the assumption that the

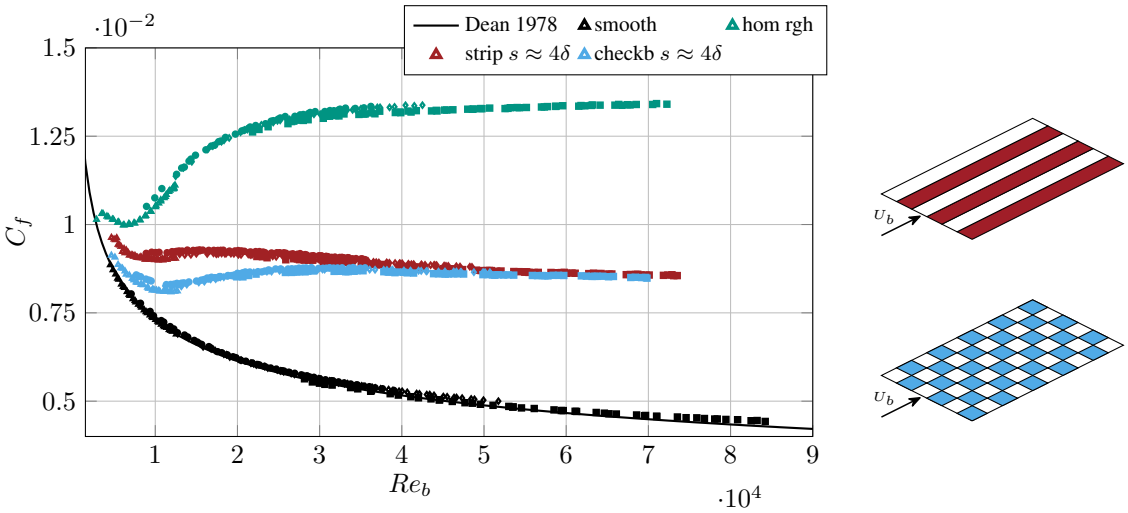

Figure 4: Friction coefficient C_f of the heterogeneous surfaces, *i.e.* 4δ-striptype and checkerboard surface as a function of Re_b, in addition the two homogeneous reference curves.

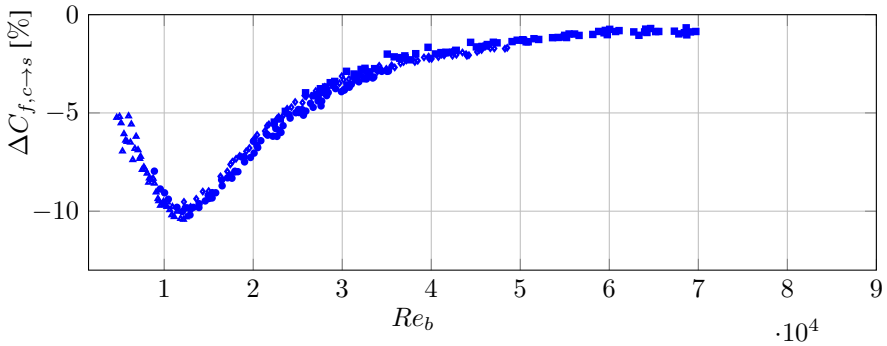

Figure 5: Relative drag change of the checkerboard pattern in comparison to the striptype surface.

influence of the channel's side walls is negligible. The resulting velocity map is shown in a contour plot in Figure 6. The measurement covers two strip widths in spanwise direction, with the rough strip placed in the middle of the white trapezium from $z/\delta = 2$ to $z/\delta = 6$. As the highest elevation of the sandpaper grain is above the smooth surface part (placed at the same mean height as the sandpaper), the wall distance is increased above the rough surface part to ensure the wire not to touch the surface, resulting in the white space in the velocity map. The measured velocity values are normalized by the channel's bulk velocity $U_{b,\dot{m}}$ which is calculated from the measured mass flow rate, whilst the geometric positions are normalized by the half channel height δ.

Lines of constant streamwise mean velocity, so-called isovels, are drawn in black, except for the line depicting $U/U_{b,\dot{m}} = 1$ which is marked in red. A bulging of the iso-lines is present up to the channel centreline ($y/\delta = 1$), especially close to the edges of the rough strips. From earlier studies it is known that this bulging is an imprint of turbulent secondary motions which form at the spanwise transition from smooth to rough and *vice versa* (Frohnapfel *et al.* (2024)). Turbulent secondary motions are known to be strongest for strip-spacing in the order of δ. The present results show that strips of width $4\,\delta$ result in a flow field that is still strongly influenced by the secondary motions such that the assumption of a local equilibrium is not expected to be valid for this flow condition.

The flow above the checkerboard pattern is investigated by means of volumetric Shake-the-Box (STB) measurements. The present results depicted in Figure 7 focus on the evaluation of the time-averaged streamwise velocity at different locations above the surface. The two top subfigures show wall normal slices at two different spanwise positions, on the left above the smooth patch, on the right above the rough patch. The mean flow direction is from left to right. A comparison of the two velocity fields shows similar flow fields far away from the wall, whilst they differ close to the wall. The flow above the rough surface patch is slower than above the smooth patch, but this difference is limited to $y/\delta < 0.15$. This observation can also be seen in the two wall-parallel slices in the bottom of the figure. The left is at the closest wall position of the measurement volume, the right one at the farthest. The difference of the velocities over the smooth and the rough surface parts is in the order of $10\,\%$ close to the wall. With increasing wall

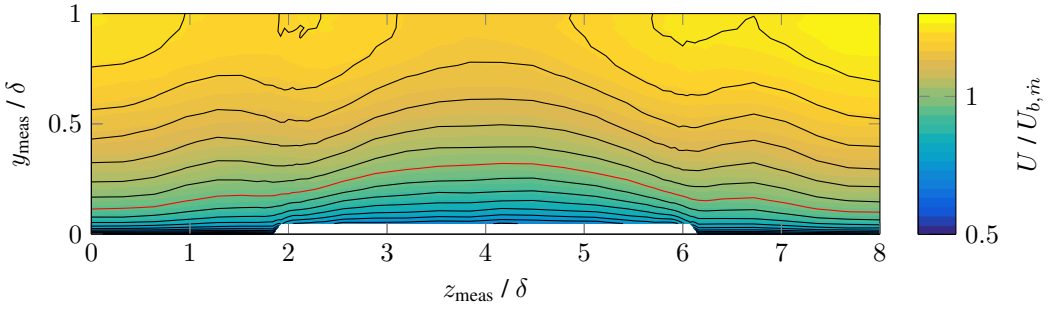

Figure 6: Streamwise velocity distribution at $Re_b = 18000$ in the channel above the $4\,\delta$ striptype surface, measured with a single hot wire. Results are normalized by half-channel height δ and the channel's bulk velocity U_b, obtained from the instantaneous mass flow rate. Black lines are isovelocity lines, the line depicting $U/U_b = 1$ is marked in red.

distance, this difference decreases, and thus is not visible anymore in subfigure d). These observations are indicators for the formation of internal boundary layers which are in equilibrium with the underlying surface after a step change in surface condition, while the outer flow is not yet affected by the new condition.

5 Discussion and Conclusions

The presented work shows the influence of the discrete arrangement of the smooth and rough surface parts of heterogeneously rough surfaces. The friction coefficient of two heterogeneous surfaces, both with $50\,\%$ roughness coverage, is investigated in an experimental campaign in a blower-type wind tunnel. The influence of the Reynolds number on the global friction coefficient is investigated over a wide Reynolds number range. In the high Reynolds number regime, the two surfaces exert the same drag on the flow. We hypothesize that this agreement is reached since the flow above the checkerboard pattern reaches a similar state as over the strip-type pattern and global drag is governed by this flow condition. This suggests that the growth rate of the internal boundary layers and the development length of turbulent secondary motions (which are a distinct feature of strip-type roughness) scale in viscous units. At larger Re_b the viscous length scale decreases such that $4\,\delta$ corresponds to a larger fetch in viscous units. In the low Reynolds number regime, a "drag reduction" effect of the roughness arranged in a checkerboard pattern in comparison to the strip-type surface is observed. This observation might be related to local under- or overshoots of local wall shear stress during the inner boundary layer development. However, we would expect these effects to roughly cancel each other on a global level. Further insights into this issue might be obtained with low Reynolds number DNS in which the local wall shear stress development is accessible.

Another possible reason for the "drag reduction" effect might be that the checkerboard pattern introduces near-wall spanwise flow when the oncoming flow over a smooth patch tries to avoid the rough surface section and is thus deflected sideways. Further analysis of the STB data will aim at investigating whether such an effect can be seen in the data. If such a spanwise motion is present, flow channelling along the smooth surface parts might lead to lower global drag. As a result near-wall streamlines would carry a slight wavy motion. A particular flow control technique, namely travelling waves of spanwise wall motion (Quadrio *et al.* (2009)), aims at introducing such near wall flow and is known to result in drag reduction. One possible passive realization of such a flow control scenario is given by wavy riblets (Cafiero *et al.* (2024)) whose optimal streamwise wave-length is in the order of $\lambda_x^+ = 1500$. Interestingly the viscous length of a checkerboard-square is in a similar order of magnitude at $Re_b \approx 12000$ where maximum "drag reduction" is observed in the present study. The checkerboard surface might thus be a passive realization of a travelling wave. Further work is needed to test this hypothesis.

Acknowledgments

Financial support by the Deutsche Forschungsgemeinschaft (DFG, German Research Foundation), project number 521110788, and the Struktur- und Innovationsfonds Baden-Württemberg (SI-BW, structural and innovation funds of Baden-Wuerttemberg) for the laser-optical measurement equipment is gratefully acknowledged. In addition, PS acknowledges support through the Alexander von Humboldt Foundation.

References

Anderson, W., Barros, J. M., Christensen, K. T. & Awasthi, A. (2015), Numerical and experimental study of mechanisms responsible for turbulent secondary flows in boundary layer flows over spanwise heterogeneous roughness, *J. of Fluid Mech.*, Vol. 768, pp. 316 - 347

Bou-Zeid, E., Anderson, W., Katul, G. and Mahrt, L. (2020), The persistent challenge of surface heterogeneity in boundary-layer meteorology: A review, *Boundary-layer Meteorology*, Vol. 177, pp. 227-245

Cafiero, G., Amico, E. and Iuso, G.(2024), Manipulation of a turbulent boundary layer using sinusoidal riblets, *J. of Fluid Mech.*, Vol. 984, A59

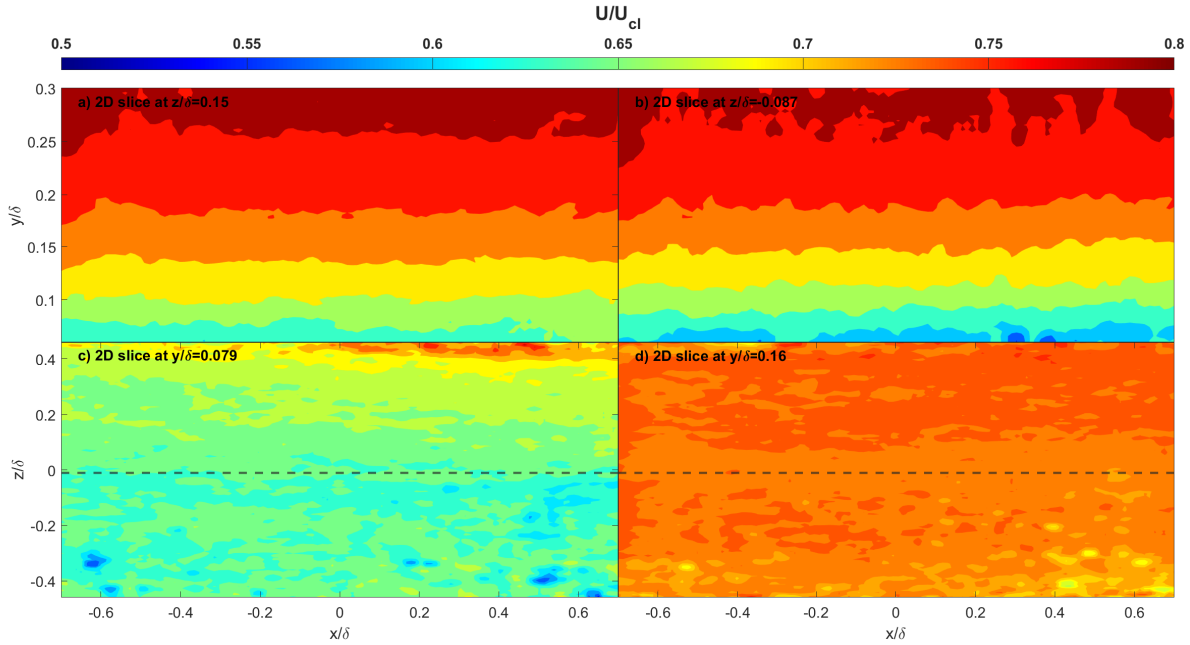

Figure 7: Results from the STB measurements. Bulk velocity normalized by centreline velocity (U/U_{cl}). Wall-normal 2D slices at spanwise (z) positions over the smooth (a) and rough (b) patches, and 2D spanwise slices at two wall-normal (y) positions over the full streamwise direction (c) $y/\delta < 0.1$ and d) $y/\delta > 0.1$). The dashed line in c) and d) represents the edge between a rough and a smooth patch.

Chung, D., Hutchins, N., Schultz, M. and Flack, K. A. (2021), Predicting the drag of rough surfaces, *Annual Review of Fluid Mechanics*, Vol. 53, pp. 439-471.

Frohnapfel, B., von Deyn, L., Yang, J., Neuhauser, J., Stroh, A., Örlü, R. and Gatti, D. (2024), Flow resistance over heterogeneous roughness made of spanwise-alternating sandpaper strips, *J. Fluid Mech.*, Vol. 980, A31.

Gatti, D., Güttler, A., Frohnapfel, B. and Tropea, C. (2015), Experimental assessment of spanwise-oscillating dielectric electroactive surfaces for turbulent drag reduction in an air channel flow, *Exp. in Fluids*, Vol. 56 (5), 110

Hehner, M. T., Coutinho, G., Santos Pereira, R. B., Nicolas Benard, N. and Kriegseis, J. (2023), On the interplay of body-force distributions and flow speed for dielectric-barrier discharge plasma actuators, *J. Phys. D: Appl. Phys.*, Vol. 56, 37

Hinze, J. O. (1967), Secondary currents in wall turbulence, *Phys. Fluids*, Vol. 10, pp. 122-125

Hutchins, N. , Ganapathisubramani, B., Schultz, M. P. and Pullin, D. I. (2023), Defining an equivalent homogeneous roughness length for turbulent boundary layers developing over patchy or heterogeneous rough surfaces, *Ocean Engineering*, Vol. 271, pp. 179 - 203

Kriegseis, J., Leister, R., Rockstroh, T., Beslać, R. and Frohnapfel, B. (2024), Turbulent channel flow diagnostics by means of Shake-the-box (STB): Flow structures and sublayer profiles, *Proceedings to 21th International Symposium on Application of Laser and Imaging Techniques to Fluid Mechanics*

Neuhauser, J., Schäfer, K., Gatti, D. and Frohnapfel, B. (2022), Simulation of turbulent flow over roughness strips, *J. Fluid Mech.*, Vol. 945, A14.

Neuhauser, J., Schmidt, C., Gatti, D. and Frohnapfel, B. (2025), Predicting the global drag of turbulent flow over roughness strips, *Internat. J. of Heat and Fluid Flow*, Vol. 115

Novara, M., Schanz, D. and Schröder, A. (2023), Two-pulse 3D particle tracking with Shake-The-Box, *Exp. in Fluids*, Vol. 64, 93

Örlü, R. and Vinuesa, R. (2017), Thermal anemometry, In *Experimental Aerodynamics* (ed. S. Discotti & A. Ianiro), pp. 257-304, CRC Press

Quadrio, M., Ricco, P. and Viotti, C. (2009), Streamwise-travelling waves of spanwise wall velocity for turbulent drag reduction, *J. of Fluid Mech.*, Vol. 7, 240

Pasch, S., Leister, R., Gatti, D., Örlü, R., Frohnapfel, B. and Kriegseis, J. (2024), Measurement in a turbulent channel flow by means of an LDV profile sensor, *Flow, Turbulence and Combustion*, Vol. 113 (1), pp. 195-213

Schanz, D., Gesemann, S. and Schröder, A. (2016), Shake-The-Box: Lagrangian particle tracking at high particle image densities, *Exp. in Fluids*, Vol. 57(5), 70

Wangsawijaya, D. D., Baidya, R., Chung, D., Marusic, I. and Hutchins, N. (2020), The effect of spanwise wavelength of surface heterogeneity on turbulent secondary flows, *J. of Fluid Mech.*, Vol. 894, A7